IEEE Access
Multidisciplinary ⋮ Rapid Review ⋮ Open Access Journal

Received December 27, 2019, accepted January 5, 2020, date of publication January 10, 2020, date of current version January 23, 2020.

Digital Object Identifier 10.1109/ACCESS.2020.2965581

One Novel Distributed Space Telescope With Payload Formation

QING LI[1], LEI LIU[1], AND JUN SHEN[2]
[1]Shaanxi Aerospace Flight Vehicle Design Key Laboratory, School of Astronautics, Northwestern Polytechnical University, Xi'an 710072, China
[2]Xi'an Institute of Space Radio Technology, Xi'an 710000, China

Corresponding author: Lei Liu (leiliu@nwpu.edu.cn)

This work was supported in part by the National Natural Science Foundation of China (NSFC) under Grant 51675430 and Grant 11402044, and in part by the Synergy Innovation Foundation of the University and Enterprise for Graduate Students in Northwestern Polytechnical University under Grant XQ201902.

ABSTRACT Large aperture space technology is critical for next-step astrophysics missions with high resolution requirement. The distributed telescope has been proven as an appealing solution to break the technical limitation in obtaining large apertures. However, the stringent interference imaging condition puts forward extremely high control accuracy requirement on the distributed telescope which is still a challenge task and need to be further studied. This paper thus presents one distributed space telescope with payload formation by synthesizing the non-contact electro-magnetic actuators. The distributed optical apertures are connected by using the deployed mechanical structure while the non-contact actuators are further employed for high precision payload formation. Large equivalent aperture is obtained due to the achievable long baseline configuration, in addition, the ultra-high control accuracy of the distributed telescope is guaranteed. The dynamics modeling and the corresponding control strategy are also provided. The effectiveness of the proposed distributed space telescope is evaluated using simulation studies.

INDEX TERMS Astrophysical investigation, distributed telescope, interference imaging, payload formation.

I. INTRODUCTION

The urgent quest for larger aperture space telescopes with high angular resolution is driven by a number of upcoming scientific missions for astrophysical investigation [1]–[3]. Unfortunately, the mirror diameter for space telescopes is limited by current technology, scaling laws of manufacturing costs, as well as volume and mass constraints of current launch vehicles [4], [5]. There still presents unique challenges due to the existing technology gap between the current state-of-art and the large aperture space optics required to enable planned astrophysics missions.

Efforts are ongoing to meet the challenges by employing exotic technologies, such as deployed segmented mirror telescopes, and distributed optics using interferometry [6]–[8]. The deployed segmented mirror technology has grown out of the quest for larger aperture and higher angular resolution on the basis of traditional monolithic-mirror telescopes [9], [10]. The James Webb Space Telescope (JWST), which adopts the deployed segmented architecture, is built to capture the first and farthest galaxies [11]. A 6.5-meter primary mirror is obtained by equipping with 18 hexagonal beryllium segments. The segmented mirror is stowed for launch and deployed after launch. The resolution of JWST is designed better than 100 milli-arcsecond (mas) [12]. For the next step, the 9.2m and 16.8m Advanced Technology Large-Aperture Space Telescope (ATLAST) mission concepts are proposed mainly rely on the deployable segmented concept from the JWST [13], [14]. The deployed segmented mirror technology utilizes the segmented mirror array to act as a single mirror, which effectively extends the achievable aperture of the traditional imaging telescope.

Monolithic mirror with large diameter is avoided, offers the advantages of achievable manufacturing process and allowable packaging configurations. On the other hand, there is added difficulty in accurately deploying and phasing individual mirror segments to achieve a phased primary mirror with desirable optical quality [13], [15], [16]. The additional actuation and control systems are required for each segment. The number of segmented mirrors, i.e., the accessibility aperture, is thus severely limited because of the increasing wavefront control complexity, system volume and mass.

The associate editor coordinating the review of this manuscript and approving it for publication was Jinguo Liu.

To further improve the aperture and angular resolution, the distributed optics using interferometry has been proposed as an ideal solution [5], [17]. The improvement of the optics aperture can be equivalent to the increase of the interferometer baseline of distributed optical components. One of the primary distributed optics is the formation flying architecture which is characterized by long achievable baseline [18]. The distributed optical components are carried by precise formation spacecraft with specific configurations. This arrangement can make available baselines up to hundreds of meters for the general astrophysics program [19]. Both the Darwin and the Terrestrial Planet Finder formation flying Interferometer (TPF-I), aiming to find and characterize earth-like planets orbiting other stars, are proposed on the basis of the distributed formation flying technology [20], [21].

For perfect interference, the formation flying spacecraft must carefully maintain the relative position and pointing to meet the stringent interference requirements [22]. The distributed optics are necessarily to be phased within a fraction of the observing wavelength [23]. This extremely stringent requirement poses a challengeable precision demand on formation flying spacecraft. In addition, the position and attitude of the distributed spacecraft need to be constantly adjusted to maintain the formation configuration. However, current spacecraft formation flying is generally implemented by using jet-propelled control, it is difficult to achieve such a high precision control while large amount of propellant is required [24]. A large amount of onboard propellant consumption greatly reduces the system operating life [25]. The operational orbit of distributed formation flying optics mission is generally designed near the second Sun-Earth Lagrange point for simpler formation-maintaining control [26]. The distributed formation flying technology is consequently identified more suitable for high orbit optical system.

In order to obtain a large aperture space telescope with better adaptable and less control complexity. This paper thus proposed a novel distributed space telescope with payload formation by using the non-contact electro-magnetic actuator. The distributed optical components are connected by employing the deployed mechanical structure which provides a long baseline configuration for the distributed telescope. The payload formation of the distributed optical components is further implemented to guarantee the interference imaging requirement by using non-contact electro-magnetic actuators. The non-contact actuators can also physically isolate the support disturbance [27]–[29]. The requirements on long baseline and high precision control are simultaneously satisfied by integrating the deployed structure with payload formation. The baselines of the proposed novel telescope architecture would lie between the deployed segmented mirror telescopes and distributed formation flying optics.

Compared to the deployed segmented concept from JWST, the proposed distributed telescope with payload formation can realize larger aperture without the need for complicated and costly deployment and control system.

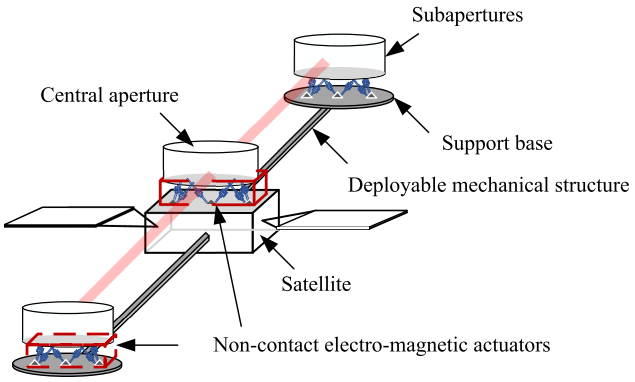

FIGURE 1. Diagram of the proposed distributed space telescope with payload formation. The configuration with one central aperture and two subapertures is taken as an example.

Furthermore, the distributed optical components of the proposed architecture are connected by using the deployed structure, the additional formation-maintaining control is avoided comparing with the formation flying optics [25], [30]. The consumption of the onboard propellant is significantly reduced to allow for various orbital environment without specific restriction. Better mobility is also obtained because of the deployed connected architecture, which is able to handle a need for faster imaging or repointing maneuver. In addition, the proposed distributed telescope guarantees an ultra-high precision control by implementing payload formation flying with non-contact actuators. The requirements on spacecraft and deployed structure are thus significantly reduced which is conducive to the reduction of system cost and technical difficulty.

This paper is organized as follows. First, the design of the novel distributed space telescope with payload formation is proposed in Section II. Then, the dynamics modeling and control strategy of the distributed telescope are provided in Section III and IV, respectively. Additionally, in Section V, the simulation studies are given to demonstrate the effectiveness of the proposed distributed space telescope. Finally, the discussion is given in Section VI and the conclusion is made in Section VII.

II. DESIGN OF THE NOVEL DISTRIBUTED SPACE TELESCOPE WITH PAYLOAD FORMATION

A novel distributed space telescope with payload formation is proposed in this paper. The system design scheme is demonstrated as shown in Fig. 1, the configuration with one central aperture and two subapertures is taken as an example. The optical apertures are arranged in a certain way according to the distributed configuration design. The satellite with deployed mechanical structure serves as the support base for the long baseline distributed telescope. The distributed optical apertures and the satellite are separated bodies that interact through the non-contact electro-magnetic actuators. The payload optical apertures are controlled to maintain the high precision formation by using the non-contact actuators.

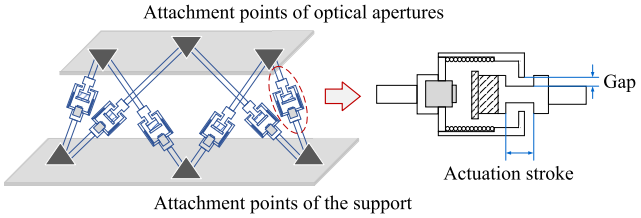

FIGURE 2. Configuration of the non-contact connection interface.

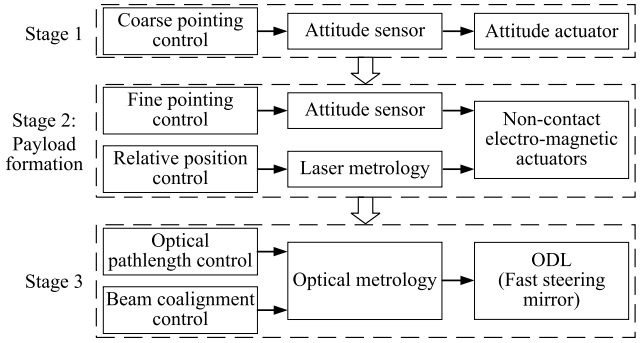

FIGURE 3. Staged measurement and control strategy of the system.

The relay optics and the beam combiner are integrated into the central aperture. The light collected by subapertures is further corrected by the relay optics and finally recombined inside the beam combiner for interferometric imaging.

The detailed configuration of the non-contact connection interface between the payload optical apertures and support base is presented in Fig. 2. Each optical aperture interacts with the support base through six non-contact electromagnetic actuators. The non-contact connection interface is designed as a 6-struts Stewart platform with cube configuration. The payload optical aperture is mounted in the upper plate through attachment points, while the support is connected with the lower plate. The apertures and support are preferably mechanically decoupled. The gap design of the non-contact actuator requires a trade-off between the required stroke of the optical apertures and the drive linearity of the non-contact actuators.

The distributed space telescope necessitates phasing of the subapertures to within a fraction of a wavelength to realize interference imaging requirement. The quest for cophasing requirement, also referred to as the optical path differences (OPD) requirement, implies a very precise control of the relative positioning control of different optical apertures. Moreover, another major requirement is beam coalignment which implies a very precise attitude control of different optical apertures. According to the proposed distributed space telescope with payload formation, the corresponding staged measurement and control strategy is also designed in this paper to meet the extremely high control accuracy. The measurement and control strategies are illustrated in Fig. 3. First, the coarse pointing control of the distributed telescope is realized by satellite attitude control with commercial attitude actuators, such as reaction wheels. Then, the pointing and relative position of the optical apertures are controlled for high precision payload formation by employing the non-contact electro-magnetic actuators. The attitude and the relative position control of the apertures rely on the attitude sensor and laser metrology, respectively. Finally, the optical delay line (ODL) control using piezoelectric fast steering mirror (FSM) is implemented to compensate the residual OPD and beam coalignment error relying on accurate optical metrology.

The proposed distributed space telescope is designed as a unitary structure, the basic configuration of the distributed apertures is guaranteed. The payload formation by using non-contact actuators is implemented which provides a solution to the problem of extremely stringent cophasing requirement. The structure thermal deformation, the deployment error, the control error of the satellite as well as the support disturbance are eliminated by introducing the non-contact actuators. The fine attitude and relative position control of the distributed apertures is guaranteed. The requirements on satellite and deployed mechanism are thus significantly relaxed. The conventional satellite can meet the system requirement without the need for ultra-precise satellite control. In the meantime, the stiffness requirement of the deployed structure is also much reduced compared to traditional structurally connected architecture, which is conducive to the reduction of the system mass. The distributed space telescope with payload formation facilitates a long optical baseline design with better mobility. The proposed design scheme is more suitable for the optical system with a baseline smaller than 100m due to the mass and volume constraints of current vehicles as well as the manufacturing limitation. In addition, the flexibility of in-orbit reconfiguration is limited comparing with formation flying telescope since the configuration of the proposed distributed telescope is relatively fixed.

III. DYNAMICS MODELING OF THE DISTRIBUTED SPACE TELESCOPE

This section presents the dynamics modeling of the proposed distributed space telescope system. The deployed structure, coupling the apertures dynamics, is taken into consideration and assumed as massless spring-damping system. Both the satellite, the optical apertures, and the support base are regarded as rigid bodies. The dynamics of the distributed space telescope is derived in the case of small angle motion assumption.

A. DYNAMICS MODELING OF THE CENTRAL APERTURE

The dynamics modeling of the central aperture is presented at first. The control of the central aperture is performed by employing six non-contact actuators as illustrated in Fig. 2. The central aperture is mounted on the upper plane as the payload unit, while the satellite body is considered as the

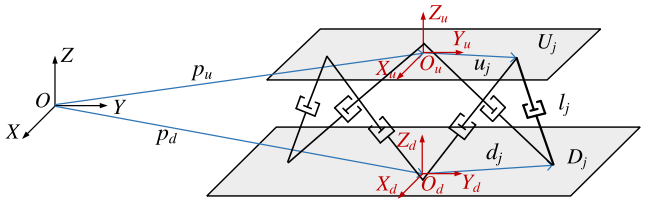

FIGURE 4. Definition of the corresponding coordinate frames.

support unit. The definition of corresponding coordinate frames is illustrated in Fig. 4.

OXYZ represents the inertial reference frame, which is assumed to coincide with the satellite orbit frame in this paper. $O_uX_uY_uZ_u$ and $O_dX_dY_dZ_d$ are coordinate frames fixed at the payload central aperture and support satellite, with origins O_u and O_d at their center of mass, respectively. Both the O_uZ_u and O_dZ_d are perpendicular to their mounting plane. U_j and D_j denote the connection hinge points of the actuating strut j to the upper and lower plane, respectively. The generalized coordinates of the payload central aperture and the support satellite in the inertial reference frame are recorded as $\boldsymbol{\chi}_u = (x_u, y_u, z_u, \alpha_u, \beta_u, \gamma_u)^T$ and $\boldsymbol{\chi}_d = (x_d, y_d, z_d, \alpha_d, \beta_d, \gamma_d)^T$, respectively.

The Jacobian matrix of the payload central aperture and support satellite are calculated as

$$\boldsymbol{J}_u = \begin{bmatrix} \cdots & \cdots \\ \tilde{\boldsymbol{l}}_j^T & \left(\boldsymbol{u}_j \times \tilde{\boldsymbol{l}}_j\right)^T \\ \cdots & \cdots \end{bmatrix}, \quad \boldsymbol{J}_d = \begin{bmatrix} \cdots & \cdots \\ \tilde{\boldsymbol{l}}_j^T & \left(\boldsymbol{d}_j \times \tilde{\boldsymbol{l}}_j\right)^T \\ \cdots & \cdots \end{bmatrix}, \quad (1)$$

where $\tilde{\boldsymbol{l}}_j$ is the unit direction vector of the actuating strut j represented in coordinate frame $OXYZ$. $\boldsymbol{u}_j$ denotes the position vector of point U_j represented in coordinate frame $O_uX_uY_uZ_u$, and $\boldsymbol{d}_j$ denotes the position vector of point D_j represented in coordinate frame $O_dX_dY_dZ_d$ as shown in Fig. 4. Considering the small angle motion assumption, the velocity of the actuating strut j can derived as

$$\dot{\boldsymbol{l}} = \boldsymbol{J}_u\dot{\boldsymbol{\chi}}_u - \boldsymbol{J}_d\dot{\boldsymbol{\chi}}_d, \quad (2)$$

The payload central aperture is driven and mechanically decoupled with the support satellite by using six active struts. There is no mechanical stiffness across the connection interface. The mass of the active struts is also neglected because the strut mass is much smaller compared to the payload aperture. The axial output force of the active strut j is given as

$$f_j = f_{cj} - f_{ej}, \quad (3)$$

where f_{cj} is the control force of the non-contact electromagnetic actuator j, and f_{ej} denotes the damping force introduced by back electromotive force. Ignoring the actuator inductance, f_{cj} and f_{ej} can be calculated according to the electric equation of the actuator as

$$f_{cj} = \frac{k_f u_{cj}}{R}, \quad f_{ej} = \frac{k_e k_f}{R}\dot{l}_j, \quad (4)$$

where k_f and k_e are electromagnetic force constant and back e.m.f. constant, respectively. u_{cj} is the control voltage of actuator j, R represents the actuator resistance. $\dot{l}_j$ is the axial velocity of the actuating strut j. Equation (3) is rewritten to

$$f_j = \frac{k_f u_{cj}}{R} - c\dot{l}_j, \quad (5)$$

where c denotes the equivalent damping coefficient of the actuator, and $c = \frac{k_e k_f}{R}$.

Then, the output force of the system is calculated as

$$\boldsymbol{F} = \boldsymbol{F}_c - \boldsymbol{C}\dot{\boldsymbol{l}}, \quad (6)$$

where $\boldsymbol{F}_c$ is the control force of the non-contact actuators, and $\boldsymbol{F}_c = \left[f_{c1}\ f_{c2}\ \cdots f_{c6}\right]^T$. $\boldsymbol{C}$ is the equivalent damping matrix of the system, and $\boldsymbol{C} = \mathrm{diag}\left[\, c\ c\ c\ c\ c\ c\,\right]$.

Therefore, the dynamics equation of the payload central aperture can be expressed in the inertial reference frame as

$$\boldsymbol{M}_u\ddot{\boldsymbol{\chi}}_u + \boldsymbol{J}_u^T\boldsymbol{C}\boldsymbol{J}_u\dot{\boldsymbol{\chi}}_u = \boldsymbol{J}_u^T\boldsymbol{C}\boldsymbol{J}_d\dot{\boldsymbol{\chi}}_d + \boldsymbol{J}_u^T\boldsymbol{F}_c, \quad (7)$$

where $\boldsymbol{M}_u = \begin{bmatrix} m_u & \\ & \boldsymbol{I}_u \end{bmatrix}$, m_u and $\boldsymbol{I}_u$ are the mass and the inertia matrix of the payload central aperture, respectively.

In the meanwhile, the dynamics of support satellite is derived as shown in (8), in which the coupling effect of the flexible solar panels is considered [31].

$$\begin{cases} \boldsymbol{M}_d\ddot{\boldsymbol{\chi}}_d + \boldsymbol{J}_d^T\boldsymbol{C}\boldsymbol{J}_d\dot{\boldsymbol{\chi}}_d + \boldsymbol{R}\ddot{\boldsymbol{\eta}} \\ \quad = \begin{bmatrix} \boldsymbol{F}_s \\ \boldsymbol{M}_s \end{bmatrix} + \boldsymbol{J}_d^T\boldsymbol{C}\boldsymbol{J}_u\dot{\boldsymbol{\chi}}_u - \boldsymbol{J}_d^T\boldsymbol{F}_c + \begin{bmatrix} \boldsymbol{F}_d \\ \boldsymbol{M}_d \end{bmatrix} + \begin{bmatrix} \tilde{\boldsymbol{F}} \\ \tilde{\boldsymbol{M}} \end{bmatrix} \\ \ddot{\boldsymbol{\eta}} + \tilde{\boldsymbol{C}}\dot{\boldsymbol{\eta}} + \tilde{\boldsymbol{K}}\boldsymbol{\eta} + \boldsymbol{R}^T\dot{\boldsymbol{\chi}}_d = \boldsymbol{0}, \end{cases} \quad (8)$$

where $\boldsymbol{M}_d = \begin{bmatrix} m_d & \\ & \boldsymbol{I}_d \end{bmatrix}$, m_d and $\boldsymbol{I}_d$ are the mass and inertia matrix of the satellite, respectively. $\boldsymbol{R}$ represents the coupling matrix of the satellite motion and flexible vibration of the solar panels. $\boldsymbol{\eta}$ denotes the modal displacement of the solar panels, $\tilde{\boldsymbol{C}}$ and $\tilde{\boldsymbol{K}}$ are generalized stiffness and damping matrix, respectively. $\boldsymbol{F_s}$ and $\boldsymbol{M_s}$ are control force and torque of the satellite, respectively. The satellite disturbances induced by reaction flywheels are synthesized by $\boldsymbol{F_d}$ and $\boldsymbol{M_d}$. $\tilde{\boldsymbol{F}}$ and $\tilde{\boldsymbol{M}}$ represent the coupling force and torque introduced by the deployed structure, respectively. The coupling effect is regarded as disturbances of the satellite.

B. DYNAMICS MODELING OF THE SUBAPERTURES

The control of the subapertures is also performed by employing the non-contact actuators. The dynamics modeling of the payload subaperture is the same as that for central aperture. The dynamics equation of the *ith* subaperture is given as

$$\boldsymbol{M}_{ui}\ddot{\boldsymbol{\chi}}_{ui} + \boldsymbol{J}_u^T\boldsymbol{C}\boldsymbol{J}_u\dot{\boldsymbol{\chi}}_{ui} = \boldsymbol{J}_u^T\boldsymbol{C}\boldsymbol{J}_d\dot{\boldsymbol{\chi}}_{di} + \boldsymbol{J}_u^T\boldsymbol{F}_{ci}, \quad (9)$$

where $i = 1, 2 \cdots n$, n is the number of subapertures.

The lower mounting base is regarded as support unit. The dynamics equation of support unit of the subaperture is derived as

$$\boldsymbol{M}_{di}\ddot{\boldsymbol{\chi}}_{di} + \boldsymbol{J}_d^T\boldsymbol{C}\boldsymbol{J}_d\dot{\boldsymbol{\chi}}_{di} = \boldsymbol{J}_d^T\boldsymbol{C}\boldsymbol{J}_u\dot{\boldsymbol{\chi}}_{ui} - \boldsymbol{J}_d^T\boldsymbol{F}_{ci} + \begin{bmatrix} \tilde{\boldsymbol{F}}_i \\ \tilde{\boldsymbol{M}}_i \end{bmatrix}, \quad (10)$$

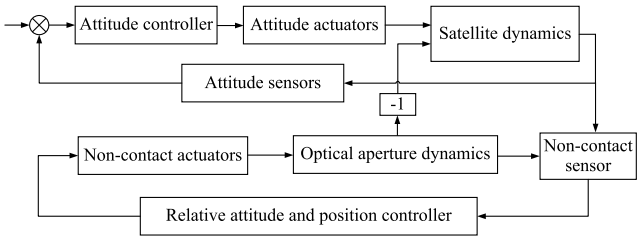

FIGURE 5. Coarse pointing adjustment of the distributed space telescope.

C. DYNAMICS MODELING OF THE DEPLOYED STRUCTURE

The coupling effect between the central aperture and the subapertures is introduced through the deployed structure. The interaction is integrated into the system as disturbance force $\tilde{\boldsymbol{F}}$ and disturbance torque $\tilde{\boldsymbol{M}}$ as demonstrated in (8) and (10). In this paper, the deployed structure is assumed as massless spring-damping system with decoupled six degrees of freedom stiffness and damping. In the meanwhile, to simplify the derivation, it is assumed that the deployed structure passes through the centroid of the satellite.

The coupling force and torque applied on the support base of the subaperture are given as

$$\begin{bmatrix} \tilde{\boldsymbol{F}}_{\boldsymbol{i}} \\ \tilde{\boldsymbol{M}}_{i} \end{bmatrix} = -\bar{\boldsymbol{K}}\Delta\tilde{\boldsymbol{\chi}}_{di} - \bar{\boldsymbol{C}}\Delta\dot{\tilde{\boldsymbol{\chi}}}_{di}, \tag{11}$$

where $\bar{\boldsymbol{K}}$ and $\bar{\boldsymbol{C}}$ are the equivalent stiffness and damping matrix of the deployed structure, respectively. $\Delta\tilde{\boldsymbol{\chi}}_{di}$ and $\Delta\dot{\tilde{\boldsymbol{\chi}}}_{di}$ are relative position and velocity between the satellite and the support unit of subaperture i, respectively.

Similarly, the coupling force and torque applied on the satellite are described as

$$\begin{bmatrix} \tilde{\boldsymbol{F}} \\ \tilde{\boldsymbol{M}} \end{bmatrix} = \sum_{i=1}^{n} \bar{\boldsymbol{K}}\Delta\tilde{\boldsymbol{\chi}}_{di} + \sum_{i=1}^{n} \bar{\boldsymbol{C}}\Delta\dot{\tilde{\boldsymbol{\chi}}}_{di} \tag{12}$$

The equivalent stiffness and damping matrix of the deployed structure can be evaluated by using finite element methods.

IV. CONTROL STRATEGY OF THE DISTRIBUTED SPACE TELESCOPE

The control strategy of the distributed space telescope with payload formation is presented in this section. The control strategy is divided into two stages considering the large angle repointing maneuver situation.

First, the coarse pointing adjustment of the distributed space telescope is carried out as shown in Fig. 5. The attitude of the satellite is controlled to achieve desired orientation by using commercial attitude actuators. In the meantime, the relative motion between optical apertures and support base is simultaneously controlled to guarantee the virtual connection stiffness by using non-contact actuators. The non-contact position sensors, which located between the two modules, are employed to obtain the relative motion information between the optical apertures and suppose base.

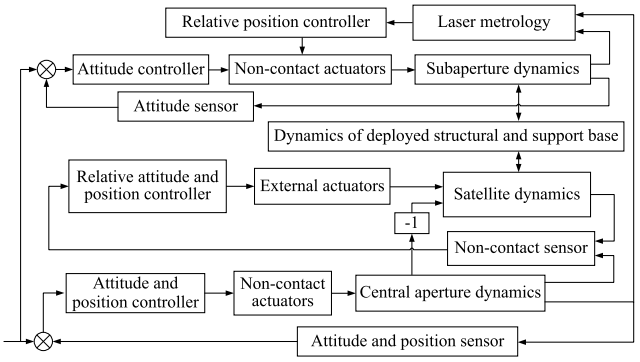

FIGURE 6. Control strategy of the payload formation flying.

The payload formation flying control is further implemented once the attitude control of satellite is stabilized. The control strategy of the payload formation flying is presented in Fig. 6. The high precision attitude and position control of the central optical aperture is implemented by using non-contact actuators while the satellite is controlled to follow the central aperture in order to keep within the range of the non-contact actuators. The attitude and relative position of each subapertures are controlled by employing the non-contact actuators to ensure accurate pointing alignment and optical path-length adjustment with central aperture. The relative position between the central aperture and subapertures are obtained by using laser metrology. The control strategy of the payload formation flying in stable pointing situation is also applicable to small angle repointing maneuver situation within actuation stroke of the non-contact actuators.

The dynamic effect of the deployed structure is considered in system control. Besides, the external disturbances and the reaction force of non-contact actuators are also taken into consideration. On the basis of the payload formation of optical apertures, the ODL control using piezoelectric multi-axis FSM is further implemented to compensate the residual OPD and beam coalignment error which is not considered in this paper.

The attitude controller of the satellite is designed as a proportional-derivative (PD) controller. The parameters of the PD controller is selected by tuning the plant into a classical second-order system with desired control bandwidth and damping rate. The control bandwidth of the satellite is limited considering the dynamic effects of the flexible solar panels and the deployed structure. Similarly, both the attitude and relative position of the optical aperture are controlled by implementing the PD control method. The design method of the PD controller is the same as that of the satellite controller.

V. SIMULATION STUDIES

The simulation studies are given in this section to evaluate the proposed distributed space telescope with payload formation. The relative position and pointing control process under disturbance and deployment error is considered.

TABLE 1. Relevant parameters of the distributed space telescope.

	Mass (Kg)	Moment of inertia (Kg·m^2)
Satellite	3560	diag([1580.5 2939.9 2954.5])
Central aperture	250	diag([56.0 56.0 70.3])
Subaperture	150	diag([33.6 33.6 42.2])
Support base of subaperture	200	diag([58.3 58.3 100])

A. SIMULATION PARAMETERS

The simulation parameters are illustrated at first. The distributed space telescope presented in Fig. 1 is taken as the simulation case. The baseline of the space telescope is designed to 60m, and the length of the two mechanical structures which connecting the subapertures is 30m. The deployed articulated truss structure is employing to provide the desired connection stiffness with relatively small mass [32]. The relevant parameters of the distributed space telescope are summarized as shown in Table 1.

The first six modal frequencies of the solar panels are taken into account, and $\boldsymbol{\Omega} = diag[1.788\ 12.932\ 15.071\ 15.487\ 37.656\ 47.003]$ (rad/s). The damping ratio ξ is designed as 0.05. Then, the generalized stiffness and damping matrix of the solar panels can be given as

$$\tilde{\boldsymbol{K}} = \boldsymbol{\Omega}^{\boldsymbol{T}}\boldsymbol{\Omega}, \quad \tilde{\boldsymbol{C}} = 2\xi\boldsymbol{\Omega} \tag{13}$$

The coupling matrix of the satellite motion and the flexible vibration of solar panels is calculated as $\boldsymbol{R} = \begin{bmatrix} \boldsymbol{R_1} \\ \boldsymbol{R_2} \end{bmatrix}$, and

$$\boldsymbol{R_1} = \begin{bmatrix} 0 & 0 & 0 & -5.16 & 0 & 0 \\ 0 & 0 & 0 & 0 & 0 & 0 \\ -4.62 & 2.39 & 0 & 0 & 1.42 & 0 \end{bmatrix} kg^{1/2}$$

$$\boldsymbol{R_2} = \begin{bmatrix} -23.66 & 5.96 & 0 & 0 & 3.20 & 0 \\ 0 & 0 & 2.19 & 0 & 0 & 0.81 \\ 0 & 0 & 0 & 24.98 & 0 & 0 \end{bmatrix} kg^{1/2} \cdot m$$

The height of the Stewart platform with cube configuration is designed to 1m. The Jacobian matrix of the payload and support units are

$$\boldsymbol{J_u} = \begin{bmatrix} 0.707 & 0.408 & 0.577 & -0.236 & -0.408 & 0.577 \\ 0 & -0.817 & 0.577 & -0.236 & -0.408 & -0.577 \\ -0.707 & 0.408 & 0.577 & 0.471 & 0 & 0.577 \\ 0.707 & 0.408 & 0.577 & 0.471 & 0 & -0.577 \\ 0 & -0.817 & 0.577 & -0.236 & 0.408 & 0.577 \\ -0.707 & 0.408 & 0.577 & -0.236 & 0.408 & -0.577 \end{bmatrix}$$

$$\boldsymbol{J_d} = \begin{bmatrix} 0.707 & 0.408 & 0.577 & -0.471 & 0 & 0.577 \\ 0 & -0.817 & 0.577 & 0.236 & -0.408 & -0.577 \\ -0.707 & 0.408 & 0.577 & 0.236 & -0.408 & 0.577 \\ 0.707 & 0.408 & 0.577 & 0.236 & 0.408 & -0.577 \\ 0 & -0.817 & 0.577 & 0.236 & 0.408 & 0.577 \\ -0.707 & 0.408 & 0.577 & -0.471 & 0 & -0.577 \end{bmatrix}$$

The equivalent damping coefficient c of the actuator is 2.5N·m/s. The stiffness and the damping matrix of the mechanical structure are given as

$$\bar{\boldsymbol{K}} = 10^2 \times diag\left[23.9\ 5.7\ 5.7\ 13.8\ 24.9\ 24.9\right]$$
$$\bar{\boldsymbol{C}} = 10^{-2} \times diag\left[1\ 1\ 1\ 1\ 1\ 1\right]$$

The PD controller is designed for satellite with control bandwidth of 0.05Hz, and the control coefficients are set to

$$\boldsymbol{k_p} = diag\left[239.3\ 291.3\ 376.0\right]$$
$$\boldsymbol{k_d} = diag\left[1077.0\ 1311.1\ 1692.5\right]$$

Similarly, the non-contact actuators are also controlled by implementing PD controller. The control bandwidth of the central aperture is set to 0.15Hz, and the control coefficients of the PD controller are designed as

$$\boldsymbol{k_{p1}} = diag\left[222.1\quad 222.1\quad 222.1\quad 49.7\quad 49.7\quad 62.5\right]$$
$$\boldsymbol{k_{d1}} = diag\left[333.2\quad 333.2\quad 333.2\quad 74.6\quad 74.6\quad 93.7\right]$$

while for the subapertures, the control bandwidth is set to 10Hz, and the control coefficients of the PD controller are

$$\boldsymbol{k_{p2}} = 10^5 \times diag\left[5.9\quad 5.9\quad 5.9\quad 1.3\quad 1.3\quad 1.7\right]$$
$$\boldsymbol{k_{d2}} = 10^4 \times diag\left[1.3\quad 1.3\quad 1.3\quad 0.3\quad 0.3\quad 0.4\right]$$

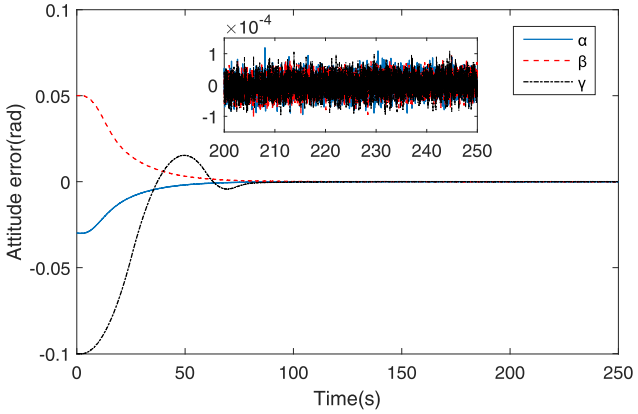

FIGURE 7. Attitude control error of the satellite.

B. SIMULATION RESULTS

Considering the repointing maneuver situation after the in-orbit deployment, the payload formation is carried out to realize the pointing adjustment of the distributed space telescope and maintain the relative position of the optical apertures. The deployment error of the subapertures, that is, the initial relative position and attitude error between the central aperture and subaperture is $[0.001\ -0.002\ 0.005\ -0.0025\ -0.001\ 0.0003]^T$(m,rad). The desired attitude of the distributed space telescope is set to $[0.05\ -0.03\ -0.1]^T$(rad).

The attitude control error of the satellite during the coarse repointing adjustment is shown in Fig. 7. The steady state attitude control error is less than 2.40×10^{-4}rad.

Figure 8 illustrates the attitude error of the support base of the subaperture. The steady state attitude control error is

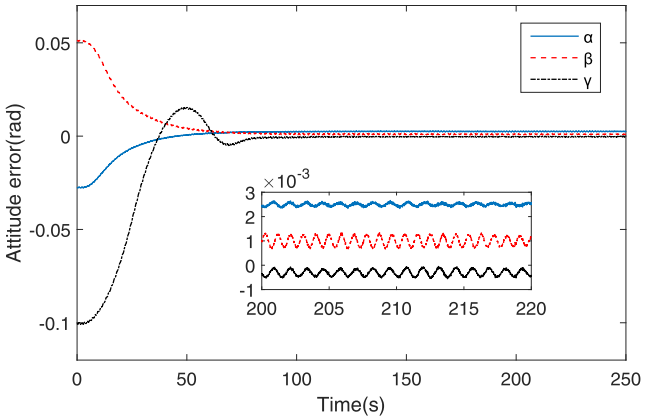

FIGURE 8. Attitude error of the support base.

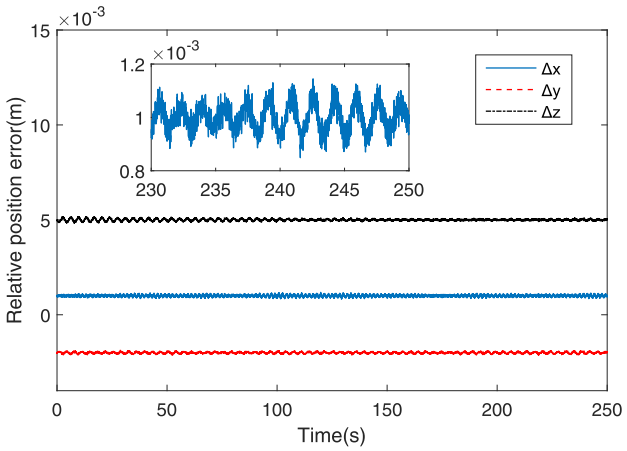

FIGURE 9. Relative position error of the satellite and support base.

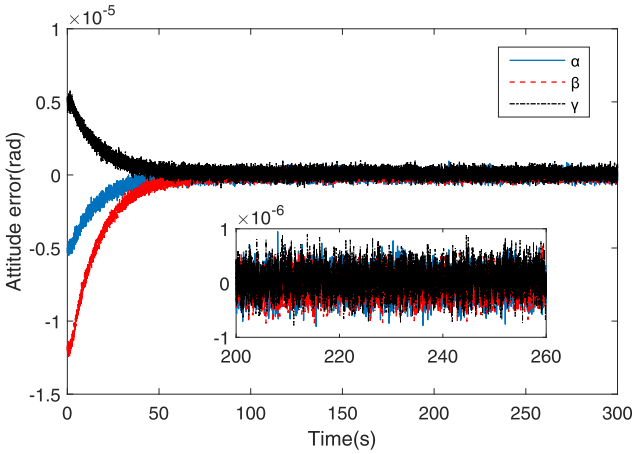

FIGURE 10. Attitude control error of the central aperture.

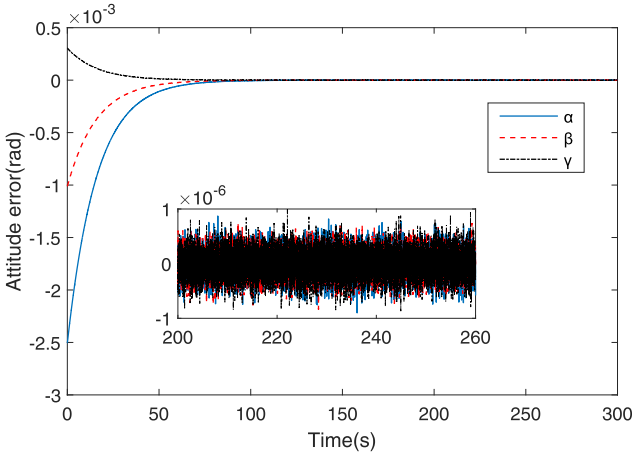

FIGURE 11. Attitude control error of the subaperture.

2.70×10^{-3} rad. The consistent movement of the satellite and support base is guaranteed relies on the rigidity of the deployed structure. However, there exists constant error component due to the deployment error. In addition, the jitter is introduced in the motion of the support base by deployed structure dynamics.

The relative position of the satellite and support base is presented in Fig. 9. The constant error component is introduced by deployment error while the jitter is caused by deployed structure dynamics. The relative position error is finally calculated as 5.30×10^{-3} m.

After the coarse repointing adjustment, the payload formation flying control is implemented to ensure accurate pointing alignment and optical path-length adjustment. Figure 10 presents the attitude control error of the central aperture, and the steady state control error is less than 1.96×10^{-6} rad. It can be seen from the results that the attitude control accuracy is improved by two orders of magnitude compared to the satellite.

Furthermore, the attitude control results of the subaperture are shown in Fig. 11 while the steady state attitude control error is less than 2.01×10^{-6} rad. The control accuracy is improved by three orders of magnitude compared to the support base. Besides, the undesirable attitude jitter is reduced by using the non-contact actuators.

The relative position error of the central aperture and subaperture is finally controlled within 2.35×10^{-6} m as shown in Fig. 12. A high precision and stable relative position control is guaranteed by using the non-contact actuators.

VI. DISCUSSION

It can be seen from Figs. 7 and 8 that the consistent movement of the satellite and support base is guaranteed relies on the rigidity of the deployed structure. The distributed configuration with long baseline is naturally maintained and the repointing maneuvers can be easily achieved.

The fine payload formation is further implemented for fine pointing and relative position control. As shown in Figs. 10 and 11, the attitude accuracy of the central aperture and the subaperture are significantly improved compared to that of the satellite and the support base. The relative position control results also demonstrate the effectiveness of the payload formation. The attitude and relative position

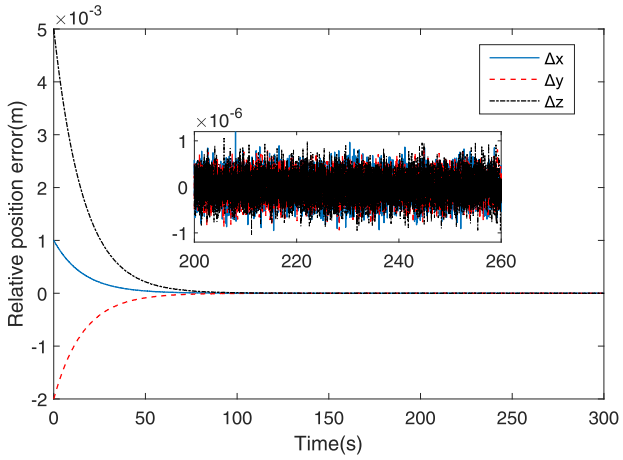

FIGURE 12. Relative position error of the central aperture and subaperture.

error of the distributed telescope are finally controlled within 2.01×10^{-6} rad and 2.35×10^{-6} m, respectively. The third-stage OPD control by using FSM is not included in this paper. Detailed studies for high precision modeling and control methods of the FSM, as well as its optical applications have been investigated in our previous paper [33], [34].

The attitude control accuracy is improved by two orders of magnitude compared to the satellite. The conventional satellite can meet the requirement without the need for ultra-precise and stable satellite control. The requirement on satellite is much reduced. Moreover, it can be seen from Figs. 11 and 12 that the deployment error and the introduced jitter are effectively compensated by using the non-contact actuators. The stringent requirement for deployment accuracy is thus released. There is less restriction on the selection of the available deployed structures which facilitates the reductions in system mass and volume.

Comparing with the distributed formation flying telescope, the deployed mechanical structure and payload formation flying are implemented to replace the satellite formation flying. The long baseline of the telescope is guaranteed while the complex formation-maintaining control is avoided and the on-board propellant consumption is much reduced. The simulation results demonstrate the effectiveness of the proposed distributed space telescope. The proposed distributed telescope with payload formation provides an alternative design approach for space telescope with ultra-high angular resolution requirement.

VII. CONCLUSION

To realize large aperture space telescope with ultra-high angular resolution, a novel distributed space telescope with payload formation flying is proposed in this paper. The payload formation flying of the distributed optical apertures is implemented by using the non-contact electro-magnetic actuators. The high precision control of the distributed telescope with micro-radian pointing accuracy and micro-meter relative position accuracy is obtained by integrating the conventional satellite with payload formation.

REFERENCES

[1] M. Postman, T. M. Brown, K. R. Sembach, J. Tumlinson, C. M. Mountain, R. Soummer, M. Giavalisco, D. Calzetti, W. Traub, K. R. Stapelfeldt, W. R. Oegerle, T. T. Hyde, Robert M. Rich, and H. P. Stahl, "Advanced technology large-aperture space telescope: Science drivers and technology developments," *Opt. Eng.*, vol. 51, no. 1, 2012, Art. no. 011007.

[2] H. P. Stahl, R. C. Hopkins, A. Schnell, D. A. Smith, A. Jackman, and K. R. Warfield, "Designing astrophysics missions for NASA's space launch system," *J. Astronomical Telescopes, Instrum., Syst.*, vol. 2, no. 4, 2016, Art. no. 041213.

[3] M. R. Bolcar, S. Aloezos, V. T. Bly, C. Collins, J. Crooke, C. D. Dressing, L. Fantano, L. D. Feinberg, K. France, and G. Gochar, "The large UV/optical/infrared surveyor (LUVOIR): Decadal mission concept design update," *Proc. SPIE, UV/Optical/IR Space Telescopes Instrum., Innov. Technol. Concepts VIII*, vol. 10398, Sep. 2017, Art. no. 1039809.

[4] M. R. Bolcar, K. Balasubramanian, J. Crooke, L. Feinberg, M. Quijada, B. J. Rauscher, D. Redding, N. Rioux, S. Shaklan, H. P. Stahl, C. M. Stahle, and H. Thronson, "Technology gap assessment for a future large-aperture ultraviolet-optical-infrared space telescope," *J. Astronomical Telescopes, Instrum. Syst.*, vol. 2, no. 4, Jul. 2016, Art. no. 041209.

[5] H. P. Stahl, "Optics needs for future space telescopes," *Proc. SPIE, Opt. Manuf. Test. V*, vol. 5180, pp. 1–5, Dec. 2003.

[6] C. Beichman, B. Benneke, H. Knutson, R. Smith, P.-O. Lagage, C. Dressing, D. Latham, J. Lunine, S. Birkmann, and P. Ferruit, "Observations of transiting exoplanets with the James webb space telescope (JWST)," *Publication Astronomical Soc. Pacific*, vol. 126, no. 946, p. 1134, 2014.

[7] A. Léger, "Strategies for remote detection of lifeąłdarwin-irsi and tpf missionsął," *Adv. Space Res.*, vol. 25, no. 11, pp. 2209–2223, 2000.

[8] N. J. Miller, M. P. Dierking, and B. D. Duncan, "Optical sparse aperture imaging," *Appl. Opt.*, vol. 46, no. 23, p. 5933, Aug. 2007.

[9] N. Lee, P. Backes, J. Burdick, S. Pellegrino, C. Fuller, K. Hogstrom, B. Kennedy, J. Kim, R. Mukherjee, C. Seubert, and Y.-H. Wu, "Architecture for in-space robotic assembly of a modular space telescope," *J. Astronomical Telescopes, Instrum., Syst*, vol. 2, no. 4, Jul. 2016, Art. no. 041207.

[10] N. Schwartz, D. Pearson, S. Todd, A. Vick, D. Lunney, and D. MacLeod, "A segmented deployable primary mirror for earth observation from a cubesat platform," in *Proc. 29th Annu. AIAA/USU Conf. Small Satell.*, Logan, UT, USA, 2016.

[11] P. A. Lightsey, C. B. Atkinson, M. C. Clampin, and L. D. Feinberg, "James webb space telescope: Large deployable cryogenic telescope in space," *Proc. SPIE, Opt. Eng.*, vol. 51, no. 1, 2012, Art. no. 011003.

[12] J. Nella *et al.*, "James webb space telescope (jwst) observatory architecture and performance," *Proc. SPIE, Opt., Infr., Millim. Space Telescopes*, vol. 5487, pp. 576–587, Oct. 2004.

[13] D. C. Redding, G. Hickey, G. Agnes, P. Eisenhardt, J. J. Green, J. Krist, L. Peterson, K. Stapelfeldt, W. Traub, M. Werner, and S. Unwin, "Active optics for a 16-meter advanced technology large aperture space telescope," Jet Propuls. Lab., Caltech, CA, USA, Tech. Rep. 7010, 2008.

[14] M. Postman *et al.*, "Advanced technology large-aperture space telescope (atlast): A technology roadmap for the next decade," 2009, *arXiv:0904.0941*. [Online]. Available: https://arxiv.org/abs/0904.0941

[15] J. L. Codona and N. Doble, "James webb space telescope segment phasing using differential optical transfer functions," *J. Astronomical Telescopes, Instrum., Syst.*, vol. 1, no. 2, 2015, Art. no. 029001.

[16] H. Peng, F. Li, S. Zhang, and B. Chen, "A novel fast model predictive control with actuator saturation for large-scale structures," *Comput. Struct.*, vol. 187, pp. 35–49, Jul. 2017.

[17] D. Defrère *et al.*, "Space-based infrared interferometry to study exoplanetary atmospheres," *Experim. Astron.*, vol. 46, no. 3, pp. 543–560, 2018.

[18] L. Massotti and E. S. Canuto, "Emerging technologies in the esa science and earth observation programme," in *Proc. IEEE Conf. Emerg. Technol. Factory Automat. (EFTA)*, Sep. 2007, pp. 69–76.

[19] C. S. Cockell, T. Herbst, A. Léger, O. Absil, C. Beichman, W. Benz, A. Brack, B. Chazelas, A. Chelli, and H. Cottin, "Darwinąłan an experimental astronomy mission to search for extra solar planets," *Experim. Astron.*, vol. 23, no. 1, pp. 435–461, 2009.

[20] C. V. M. Fridlund, "Darwin-the infrared space interferometry mission," *ESA Bull.*, vol. 103, no. 3, pp. 20–25, 2000.

[21] C. Beichman, G. Gómez, M. Lo, J. Masdemont, and L. Romans, "Searching for life with the terrestrial planet finder: Lagrange point options for a formation flying interferometer," *Adv. Space Res.*, vol. 34, no. 3, pp. 637–644, 2004.
[22] B. L. Swinkels, A. Latoui, N. Bhattacharya, A. A. Wielders, and J. J. M. Braat, "Absolute distance metrology for space interferometers," *Proc. SPIE, Recent Develop. Traceable Dimensional Meas. III*, vol. 5879, Aug. 2005, Art. no. 58790N.
[23] M. Ollivier, J.-M. Mariotti, A. Léger, P. Sékulic, J. Brunaud, and G. Michel, "Nulling interferometry for the darwin space mission," *Comp. Rendus de l'Académie des Sci.-Ser. IV-Phys.*, vol. 2, no. 1, pp. 149–156, 2001.
[24] D. P. Scharf, F. Y. Hadaegh, and S. R. Ploen, "A survey of spacecraft formation flying guidance and control. Part II: Control," in *Proc. Amer. Control Conf.*, vol. 4, Jun./Jul. 2004, pp. 2976–2985.
[25] R. L. Stephenson, Jr., and D. W. Miller, "Comparison of structurally connected and separated spacecraft architectures for the terrestrial planet finder," *Proc. SPIE, Astronomical Interferometry*, vol. 3350, pp. 672–682, Jul. 1998.
[26] O. Wallner, K. Ergenzinger, R. Flatscher, and U. Johann, "X-array aperture configuration in planar or non-planar spacecraft formation for darwin/TPF-I candidate architectures," *Proc. SPIE, Techn. Instrum. Detection Exoplanets III*, vol. 6693, Sep. 2007, Art. no. 66930U.
[27] N. Pedreiro, "Spacecraft architecture for disturbance-free payload," *J. Guid., Control, Dyn.*, vol. 26, no. 5, pp. 794–804, Sep. 2003.
[28] L. W. Sacks, C. Blaurock, L. D. Dewell, K. Tajdaran, K.-C. Liu, C. Collins, G. J. West, K. Q. Ha, M. R. Bolcar, J. E. Hylan, R. M. Bell, Jr., and J. A. Crooke, "Preliminary jitter stability results for the large UV/optical/infrared (LUVOIR) surveyor concept using a non-contact vibration isolation and precision pointing system," *Proc. SPIE, Space Telescopes Instrum., Opt., Infr., Millim. Wave*, vol. 10698, Jul. 2018, Art. no. 1069842.
[29] H. Yang, L. Liu, H. Yun, and X. Li, "Modeling and collision avoidance control for the disturbance-free payload spacecraft," *Acta Astronautica*, vol. 164, pp. 415–424, Nov. 2019.
[30] D. M. Surka and E. F. Crawley, "A comparison of structurally connected and multiple spacecraft interferometers," Tech. Rep. NASA/CR-96-207557, 1996.
[31] L. Mazzini, *Flexible Spacecraft Dynamics, Control and Guidance*. Rome, Italy: Springer, 2015.
[32] L. Puig, A. Barton, and N. Rando, "A review on large deployable structures for astrophysics missions," *Acta Astronautica*, vol. 67, nos. 1–2, pp. 12–26, Jul. 2010.
[33] Q. Li, L. Liu, X. Ma, S.-L. Chen, H. Yun, and S. Tang, "Development of multitarget acquisition, pointing, and tracking system for airborne laser communication," *IEEE Trans. Ind. Informat.*, vol. 15, no. 3, pp. 1720–1729, Mar. 2019.
[34] L. Liu, Q. Li, H. Yun, J. Liang, and X. Ma, "Composite modeling and parameter identification of broad bandwidth hysteretic dynamics in piezoelectric fast steering platform," *Mech. Syst. Signal Process.*, vol. 121, pp. 97–111, Apr. 2019.

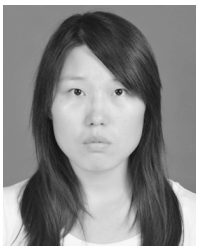

QING LI received the B.Eng. and M.Eng. degrees in flight vehicle design from the School of Astronautics, Northwestern Polytechnical University, Xi'an, China, in 2015 and 2017, respectively, where she is currently pursuing the Ph.D. degree in flight vehicle design. Her research interests include modeling, identification and control of precision motion systems, and electro-optical system control.

LEI LIU received the B.Eng. and Ph.D. degrees in aeronautical and astronautical science and technology from the Harbin Institute of Technology, Harbin, China, in 2005 and 2011, respectively, and the Ph.D. degree in electrical engineering from the National University of Singapore, Singapore, in 2012. He is currently an Associate Professor with the School of Astronautics, Northwestern Polytechnical University, Xi'an, China. His research interests include modeling, identification and control of precision motion systems, spacecraft dynamics and control, active vibration isolation, and electro-optical system control.

JUN SHEN received the B.Eng. degree in communication and information system from the China Academy of Space Technology, in 2005, and the B.Eng. degree in space science from International Space University, in 2016. He is currently an Engineer with the Xi'an Institute of Space Radio Technology, Xi'an, China. His research interests include satellite antenna and space mechanical engineering.